

Improving Snow Nowcasts for Airports

Seppo Pulkkinen, Annakaisa von Lerber,
Elena Saltikoff
Research department
Finnish Meteorological Institute
Helsinki, Finland
First.lastname@fmi.fi

Martin Hagen

Institute of Atmospheric Physics
German Aerospace Center (DLR)
Oberpfaffenhofen, Germany
First.lastname@dlr.de

Abstract—PNOWWA (Probabilistic Nowcasting of Winter Weather for Airports) project has studied methods to forecast snowfall for next few hours by extrapolating movement of radar echoes. Three different methods to create motion vectors (a simple method, a method used operationally and a new method) as well as three methods to produce probability forecasts with help of a motion vector field have been studied. The verification results of four case studies show a large dependence of the weather regime: widespread frontal precipitation is easier to forecast than isolated snow showers. The effect of orography can be split to quantitative enhancement of snowfall due to lower hills and mountains, and dynamic effect of the Alps which are affecting the movement of the entire weather system. Here the forecasts using motion extrapolation will often fail due to the complex interaction of synoptic-scale systems with orography. A further aspect in this study is the conversion of radar reflectivity (either forecasted or actual measured) to parameters which are of interest for the airport operation like visibility, de-icing index, or snow accumulation. Conversion formulas will be provided for easy use, even though there is a large uncertainty due to the wide variability of the shape and density of ice particles or snowflakes.

Keywords—snow, nowcasting, extrapolation, orography

I. INTRODUCTION

The PNOWWA (Probabilistic Nowcasting of Winter Weather for Airports) project produces methods for the probabilistic short-term forecasting of winter weather. A survey of user needs has shown demand of short, detailed forecasts (nowcasts) of snowfall and related phenomena such as the decrease of visibility, and accumulation on runways. Empirical conversion formulas will be provided, however, due to the large variability of ice particles or snowflakes there is a large scatter in the retrieved parameters.

The approach taken in PNOWWA is based on extrapolation of the movement of snowfall areas in consecutive radar images. Extrapolative methods have their limits, but in the very short range forecasting they have the ability to express timing of short-lived phenomena, such as a 45 minute pause in snowfall. Very few other methods can do that. The presence of mountains in the vicinity of airports will considerably influence the behavior of precipitation systems and thus the predictability in short time ranges. This is studied in detail for the airports of Oslo in Norway and Rovaniemi in Northern Finland. Even

more complex is the situation for the airports of Munich in Southern Germany and Salzburg in Austria where there is a strong interaction between the Alps and synoptic-scale precipitation systems.

II. NOWCASTING METHODS

A. Motion of precipitation

In a method suggested by Andersson and Ivarsson [1] the wind at 850 hPa level is used to describe the movement. The wind is taken from HIRLAM (High Resolution Limited Area Model) numerical weather prediction model. This approach had been tested in SESAR1, so it was known to provide reasonable results.

The method operationally used and originally developed at FMI, applies modified correlation-based atmospheric motion vector (AMV) system by EUMETSAT [2]. It is described in detail in [3]. The AMV system was originally developed to extract wind data from METEOSAT imagery to be used as input for numerical weather prediction. For that purpose it provides a sophisticated automatic quality indicator (QI) of the vectors [4], which is also useful in application to the radar images.

The five latest 500 m PseudoCAPPI reflectivity fields combined from ten radars in Finland are used as the input to the AMV system. Radar echoes with reflectivity less than 0 dBZ are removed from the analysis. Data is processed at time steps of 5 minutes, in grid of 16 x 16 km grid boxes. Each grid box is compared to the neighboring grid boxes from the previous time step, and the best autocorrelation is chosen to show the area of origin of the precipitation cells in the grid box.

The quality indicators of atmospheric motion vectors consist of five separate parts: consistency is tested for direction, speed, vectors, spatial homogeneity and for first guess field. The five parameters are then combined to one normalized quality indicator QI, details of this are described in [4]. In the application for radar images, vectors with quality index QI greater than 0.7 are included. This allows scatter of 1-15 degrees in direction, and 5%-20% in speed.

The PNOWWA project has received funding from the SESAR Joint Undertaking under the European Union's Horizon 2020 research and innovation programme under grant agreement No 699221

has equally large probability to arrive at the target point at the validity moment of the forecast).

In the FMI operational method the smoothed motion vector field is used “backwards” step by step: first finding out where is the pixel which should be at airport in 15 minutes, then seeing where that pixel comes from etc. Distribution of pixels in an ellipse at the source point is used to estimate the uncertainty and hence converted to probability distribution. The dimensions of the ellipse come from quality indicator of the vector field (lower quality, larger ellipse), and pixels within the ellipse get a Gaussian weighing, the pixels in the center having the largest weight.

The stochastic ensemble method can use any motion vector field as an input. It is the only method which assesses also the uncertainty due to growth and decay of the precipitation systems, not only the uncertainty in the motion field.

It is known that forecast uncertainty increases with lead time, and predictability is proportional to spatial scale (i.e. small-scale features have shorter lifetime). In the stochastic ensemble method this is modeled by autoregressive process in each spatial scale. Unexplained variance is gradually replaced with spatially correlated noise field.

Perturbations are added to the deterministic nowcast based on the motion field. 51 ensemble members are obtained by perturbing precipitation intensities and motion field. The ensemble mean represents the “most probable” precipitation intensity. The mean field becomes smoother when the forecast time increases: badly predictable scales are filtered out. The ensembles also yield probability distributions of precipitation intensities. At a given location, an empirical probability distribution for precipitation intensity can be constructed from the ensemble members.

III. VERIFICATION AS CASE STUDIES

These verification exercises are limited to comparing the nowcasts of radar reflectivity to observations of radar reflectivity. The research area was Southern Finland, and a period of 12 nowcasts at 5 min intervals were studied. Four cases were considered – radar images of all these are in Fig. 4:

- Case W is widespread precipitation 1 Feb 2015

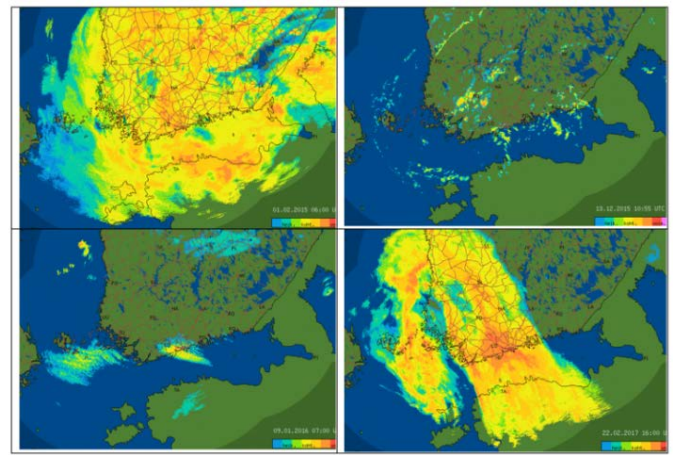


Figure 4. Radar images: from top left: Case W (1 Feb 2015), Case K (13 December 2015), Case L (9 January 2016), and Case T (22 February 2017).

- Case K was isolated snow showers 13 December 2015
- Case L was lake effect snow 3 – 9 January 2016.
- Case T was frontal precipitation 22 February 2017

The parameters selected for assessing quality of probability forecasts are Brier score, CSI and ROC. These are described in detail at website of WWRP/WGNE Joint Working Group on Forecast Verification Research or in book by Jolliffe and Stephenson [9]. Brier score answers the question: What is the magnitude of the probability forecast errors? It measures the mean squared probability error. Brier score range 0 to 1, with perfect score being 0. Brier scores for all four cases as function of forecast length are shown in Fig. 5a.

The Brier score can be decomposed into 3 additive components: Uncertainty, Reliability, and Resolution. The reliability term measures how close the forecast probabilities are to the true probabilities, given that forecast. For example, if we group all forecast instances where 80% chance of snowed was forecast, we get a perfect reliability only if it snowed 4 out of 5 times after such a forecast was issued. The resolution term measures how much the conditional probability given the different forecasts differs from the climatic average. The higher this term is the better. In the worst case, when the climatic probability is always forecast, the resolution is zero. In the best case, when the conditional probabilities are zero and one, the resolution is equal to the uncertainty.

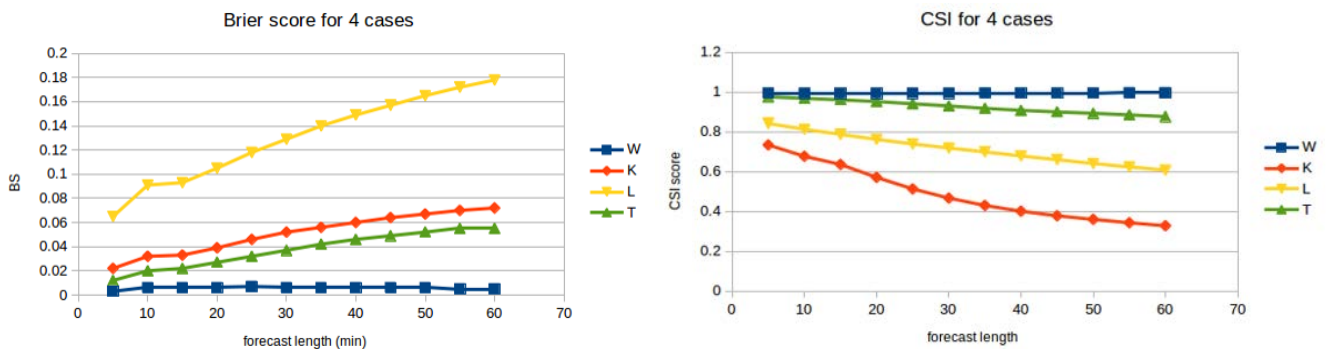


Figure 5. Brier score (left) and CSI (right). Case W (1 Feb 2015) in blue, Case K (13 December 2015) in red, Case L (9 January 2016) in yellow, and Case T (22 February 2017) in green.

In this short verification set, widespread precipitation case W gets almost perfect scores, because high probabilities are forecasted and snow is almost always observed. The lake effect case gets worst scores.

The Brier score includes comparison to climatology, which is not straightforward in comparing such disparate events. Our plan is to perform longer verification timeseries using Brier Skill Score, and the persistence as a reference forecast.

A more common verifications score, critical success index CSI, was calculated assuming that probability over 50% means "yes". The CSI measures, how well did the forecast "yes" events correspond to the observed "yes" events? CSI combines probability of detection and the false alarm rate. CSI score ranges from 0 to 1, with perfect score being 1. CSIs for all four cases as function of forecast length are shown in Fig. 5b.

From the CSI scores we can see, as expected, that the predictability in case W (widespread precipitation) is high for all forecast lengths (because in whatever direction the snowfall area moves, it is still snowing everywhere), while for case K (scattered showers) the quality decreases rapidly. The frontal precipitation case T is nearly as good as W, and the lake effect case is somewhere between showers and the others.

Relative operating characteristic ROC is presented by plotting hit rate (POD) vs false alarm rate (POFD), using a set of increasing probability thresholds (0.1, 0.2, 0.3, etc.) to make the yes/no decision. The area under the ROC curve is frequently used as a score. ROC answers the question: What is the ability of the forecast to discriminate between events and non-events? A perfect curve travels from bottom left to top left of diagram, then across to top right of diagram. Diagonal line indicates no skill. ROC curves for 60 minute forecasts are shown in Fig. 6. It is easy to see, how for widespread precipitation the probability of detection stays relatively high but also the false alarm rate is relatively high, while for the showers case false alarms are more rare.

Longer verification periods and comparison of different nowcasting methods in the same situations are still to be calculated.

IV. CONVERSION OF PARAMETERS

A. Needs for conversions

All the nowcasting methods produce probability distribution of radar reflectivity in dBZ. PNOWWA Survey indicated the parameters which are most useful for different

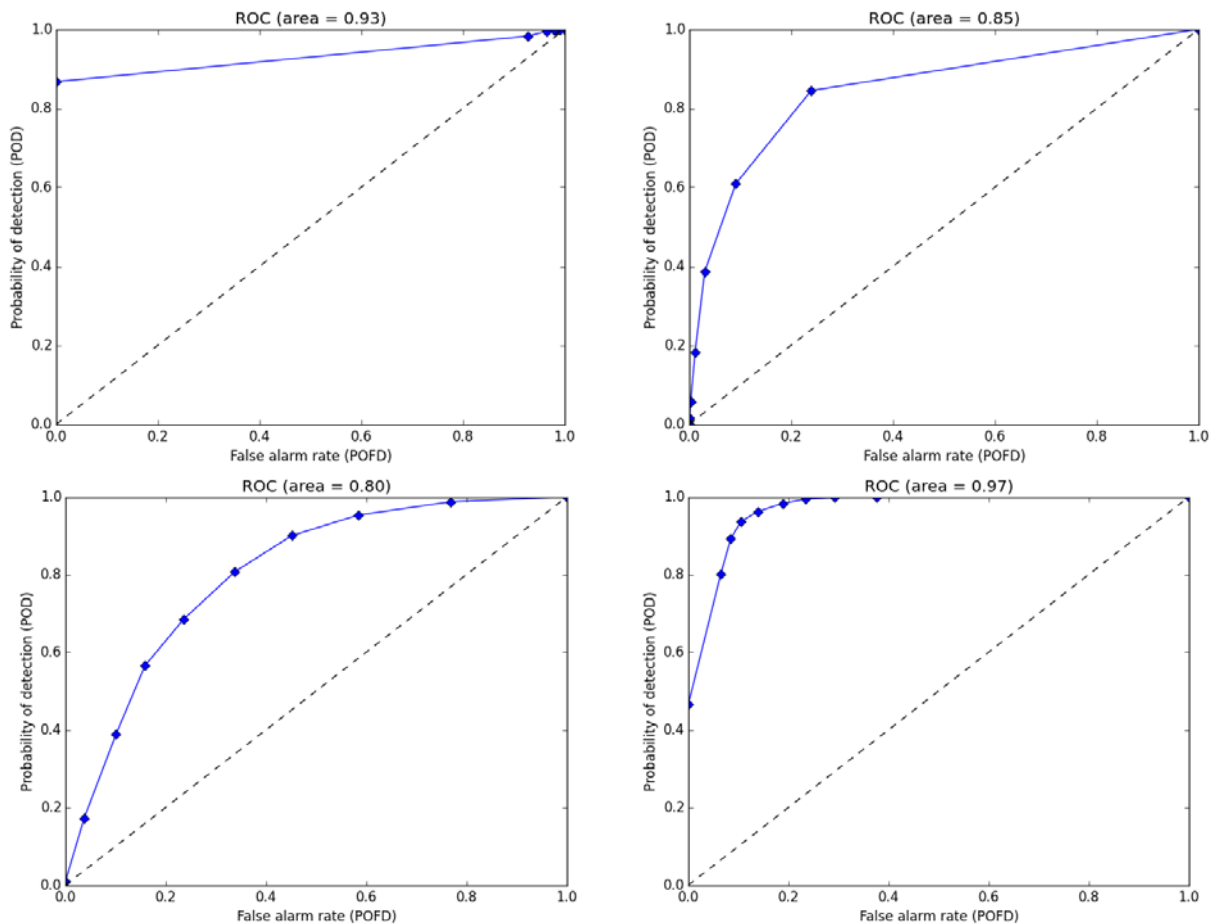


Figure 6. ROC curves for 60 minute forecasts for cases W (top left; 1 Feb 2015), Case K (top right; 13 December 2015), Case L (bottom left; 9 January 2016), and Case T (bottom right; 22 February 2017).

activities at the airport.

Several conversion equations are needed, using the reflectivity forecasts and a number of auxiliary data such as temperature and dewpoint, which are achieved from the METAR observations, TAF forecasts or HIRLAM numerical weather prediction model.

These conversion equations were used to express the user-defined parameters in radar reflectivity dBZ. The results, as used in the first scientific demo, are shown in tables 2 – 4.

The microphysical properties of different types of snowflakes are different. Some of the differences are related to temperature: ice needles fall in very cold temperatures, large “monster snowflakes” in near-zero temperatures, while wet snow is observed in even warmer weather.

To select the right dBZ thresholds, type of snow had to be determined. ICAO has defined the types of snow as follows [10]

- Dry snow – can be blown if loose or compacted by hand, will fall apart again upon release.
- Wet snow – can be compacted by hand and will stick together and tend to form a snowball.
- Compacted snow – can be compressed into a solid mass that resists further compression and will hold together, or break up into lumps, if picked up.

The most useful parameter to distinguish between snow and rain is the wet bulb temperature. Near 0°C of the wet-bulb temperature, both rain and snow are possible, and the probability of liquid rain increases with increasing wet bulb temperature. The image below (Fig. 7) shows the cumulative distribution of the non-zero rain-components as function of wet-bulb temperature, analyzed with a video-disdrometer Particle Imaging Package (PIP). As coarse analysis, it can be stated that until -0.45°C, snow can be treated as dry, with rain-component being less than 10% in the CDF and over 1.9°C, it can be treated as rain as 90% in CDF is considered to be composed of rain. In between wet snow values can be applied.

As wet bulb temperature is not included in standard METAR airport observations, the snow type for PNOWWA

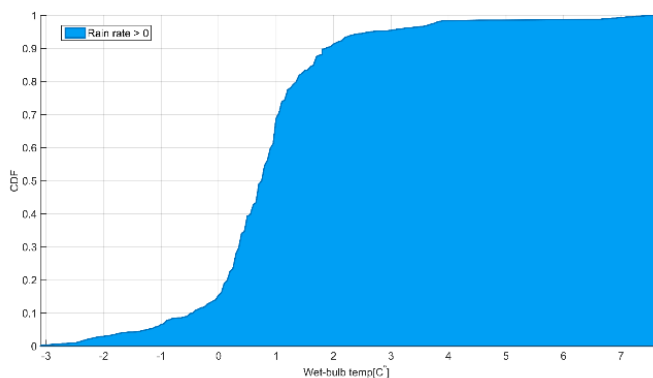


Figure 7. Cumulative distribution function of rain component of the precipitation rate higher than zero as a function of the wet-bulb temperatures.

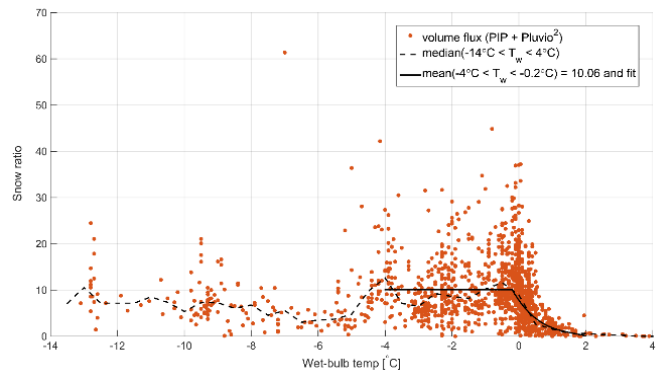


Figure 8. The 15 minute values of snow ratio for 95 snow cases, the median values calculated for every half degree bins of wet-bulb temperature between -14°C - 4°C are depicted in bracket line and solid line show the mean value of snow ratio in temperature region of -4°C – (-0.2°C) and the fit describing the change of snow ratio as function of wet-bulb temperature.

demos was determined based on temperature and dewpoint, read from the METAR.

The microphysical properties of different types of snowflakes were studied using the video-disdrometer Particle Imaging Package (PIP), OTT Pluvio² weighing gauge and laser snow depth sensor (Jenoptik SM30).

In Fig. 8 the snow ratio for every 15 minutes is plotted as function of wet-bulb temperature. The median value is computed for every half degree bin. There are only few observations of the cold snow events, and there are not enough data points to make any conclusions. The larger values such as 40 even with temperatures close to 0°C are most likely because of the low precipitation rate, when resolution accuracy of Pluvio2 accumulation might be too coarse for computing the ratio. The mean value of snow ratio, 10.1, calculated between temperatures -4°C and -0.2°C, is selected to present the snow ratio in dry snow. The polynomial third-order fit is performed in between temperatures -0.2°C and 2°C to define the ratio in wet snow. Approximately it can be assumed to be 5.

TABLE I. THE DEPENDENCY BETWEEN VISIBILITY AND RADAR REFLECTIVITY

Visibility	dBZ for dry snow	dBZ for wet snow
≤600	>29.0	>29.0
600-1500	24.5-29.0	23.5-29.0
1500-3000	15.5-24.5	19.5-23.5
>3000	<15.5	<19.5

TABLE II. THE DEPENDENCY BETWEEN LIQUID WATER EQUIVALENT AND RADAR REFLECTIVITY

Liquid water equivalent mm/h	dBZ for dry snow	dBZ for wet snow
≥4	>29.0	>29.0
2-4	24.5-29.0	23.5-29.0
0.4-2	15.5-24.5	19.5-23.5
<0.4	<15.5	<19.5

TABLE III. THE DEPENDENCY BETWEEN SNOW ACCUMULATION AND RADAR REFLECTIVITY

Snow accumulation mm/15 min	dBZ for dry snow	dBZ for wet snow
>10	>29.0	>29.0
5-10	24.5-29.0	23.5-29.0
1-5	15.5-24.5	19.5-23.5
<1	<15.5	<19.5

TABLE IV. THE DEPENDENCY BETWEEN DE-ICING WEATHER INDEX AND RADAR REFLECTIVITY

De-icing	dBZ for dry snow	dBZ for wet snow
3	>24.5	>23.5
2	15.5-24.5	19.5-23.5

B. Visibility

Both meteorological visibility and radar reflectivity are related to scattering properties of snowflakes: their size, type and amount. Still, using radar measurements for describing visibility in snowfall is a challenging task, mainly because of the strong dependence of extinction on microphysical parameters. For a given snowfall rate, the visibility has a large range of values, changing from a factor of 3 to 10 [11]. Particle size distribution has large effect on the relation between the radar reflectivity factor and the visibility. For example if the snow particle mass in the radar measurement volume stays the same, but through aggregation process the snow particles aggregate to snowflakes, the radar reflectivity increases strongly, but the visibility increases although the scattering cross-section enlarges [12], [13]. In her BSc thesis using measurements from Finland, Kaisa Ylinen found that the visibility of the same radar reflectivity factor was less than in the published studies. It can be speculated that this is because the cases she studied were in very cold weather (-10 ... -30°C), while many other researchers have mainly studied cases in near-zero temperatures, and the type of snowflakes is strongly connected to temperature [14].

Fig. 9 shows an example from visibility measurements at Munich airport using radar measurements with the DWD weather radar located at Isen about 30 to the South-East of the airport. It should be noted that the radar measurements are about 300 m above the airport and therefore not always represent the visibility observations at the surface. This might partly explain the large scatter, but a considerable part of the scatter is related to the large variability in size, density and shape of snowflakes. The parametrizations indicated in Fig. 9 refer to Table 3 in [14].

V. EFFECT OF MOUNTAINS

A. Quantitative studies

When airflow approaches or comes over mountains, snowfall is more difficult to forecast than in other situations. The predictability is worse for all studied methods:

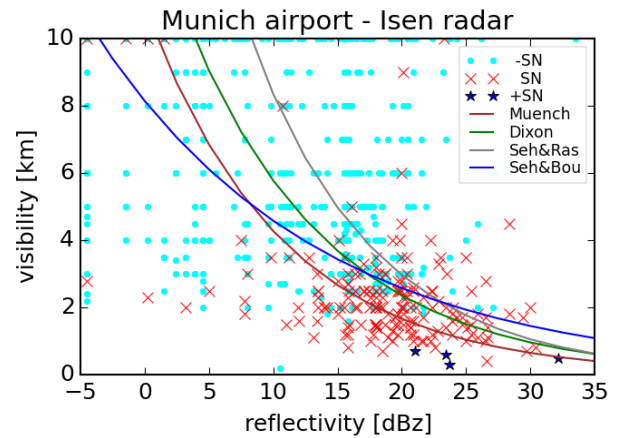


Figure 9. Visibility vs. reflectivity for Munich airport using Isen radar. Symbols indicate METAR snowfall intensities; fitting lines indicate different empirical relations [14].

extrapolation of radar images (which is the subject of PNOWWA), but also for TAF forecasts written by human forecasters, and for numerical weather prediction models.

The quantitative effect of sea and orography was estimated using the nowcasting system developed for SESAR1, which was run on additional periods. The forecasted parameter is DIW, de-icing weather, which is an index getting values 0-3. For the comparison, DIW index is calculated in three ways:

- DIW_e - Extrapolating the movement of radar echoes using the method described by [1]
- DIW_T - from TAF forecasts
- DIW_m - from HIRLAM numerical weather prediction model forecasts

The orographic effect was studied using the SESAR1 methods at two airports: Rovaniemi EFRO and Oslo Gardemoen ENGM.

Days were counted as orographic effect days if at 850 or at 925 hPa (in the case of EFRO also 950 hPa was taken into account, as the terrain and height differences are rather low there) was from the sector (180° – 250°) in Rovaniemi and from (80° – 180°) in Oslo. In most days the direction of the flow varies with time; the flow was considered coming from the valley when it remained in the sector at least two hours.

In almost all the situations, the radar-based extrapolation method (DIW_e) was slightly better than the others. Only in average of all cases for the 2 – 3 h period model forecasts outperformed the radar extrapolation. In orographic situations DIW_e was best for the whole 3-hour period. Fig. 10 shows the performance of DIW_e for Rovaniemi and Oslo. If the flow is affected by mountains forecast quality is less than for all cases.

B. Dynamical studies

For the airports of Munich (EDDM) and Salzburg (LOWS) the effect of the Alps on the behavior of cold fronts approaching from northerly directions was investigated. It is observed that cold fronts can either be delayed when approaching the Alps, other systems cross the Alpine Foreland

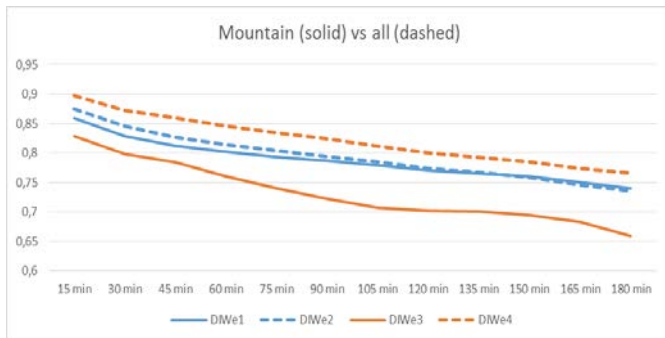


Figure 10. Summary showing the extrapolation performance in Oslo (red) and Rovaniemi (blue).

and the Alps without delay, and even acceleration can be observed for fronts passing along the Alpine Foreland (e.g. [15] or [16]). Delayed systems can generate long-lasting (up to a few days) continuous rain or snow fall events. Numerical weather forecast can forecast the behavior on a long term basis. However, nowcasting for a time horizon of one to three hours extrapolation techniques are more favorable because numerical models need some spin-up time. Radar-based extrapolation techniques will fail in case of non-linear propagation speed and direction due to delay or acceleration.

22 cases from the winters (December - March) 2013-14, 2014-15, 2015-16, and 2016-17 (April) were investigated where cold fronts did approach the Alps in the Munich/Salzburg region. To increase the number of samples both situations with rain and snowfall at ground were considered. In about half of the cases the fronts did pass the Alpine Foreland without noticeable delay (cf. Fig. 11), whereas the other cases showed considerable delay of the frontal motion leading to long lasting precipitation events (cf. Fig. 12). The

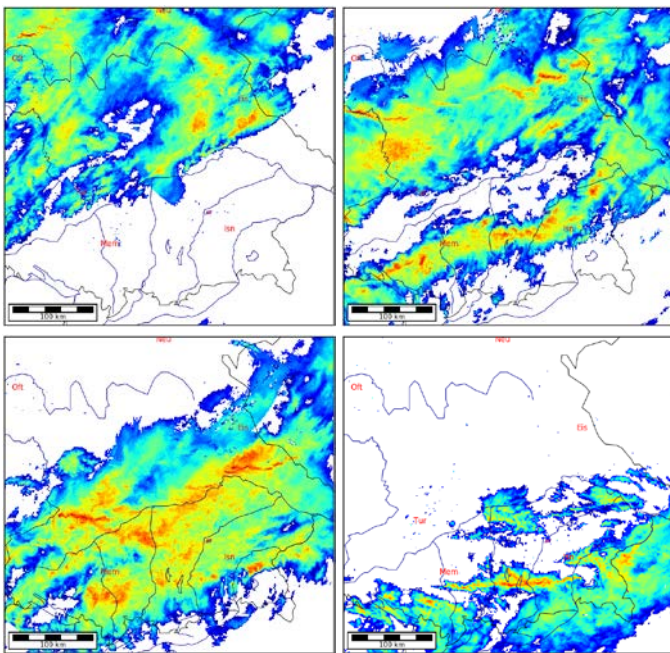


Figure 11. 3-hourly radar images of a frontal system passing South-Eastern Germany without major delay from 16 UTC on 19 until 00 UTC on 20 December 2014.

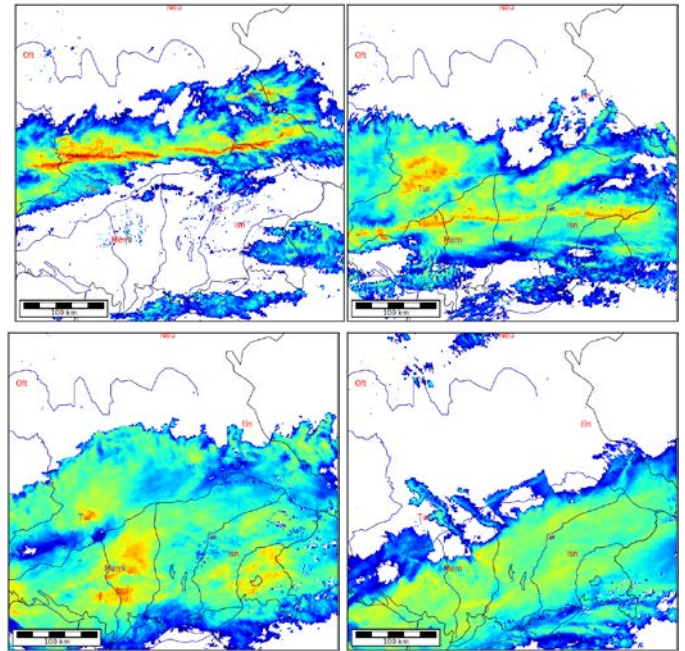


Figure 12. 3-hourly radar images of a frontal system passing South-Eastern Germany with delay and enhancement at the Alps from 22 UTC on 10 to 07 UTC on 11 January 2015.

duration of the events was between 8 and 46 hours.

Fig. 13 shows the distribution of the events in relation to the approaching direction of the frontal systems. To find relations between flow and behavior the wind profile as measured by the radio sonde München-Oberschleißheim (located in the Alpine foreland about 50 km north of the Alps) was investigated (cf. Fig. 13). However, there is no clear relation between the propagation direction of the fronts and the wind direction at the 850 and 500 hPa level (about 1000 m above the Alpine Foreland and 2 km above the main ridge). This is mainly caused by the fact that during winter when the tropopause is low the Alps act as a major obstacle and cause a considerable distortion of the atmospheric flow. Especially during those conditions which were classified as up-slope or delay often low pressure systems develop in the Alpine region causing long-lasting precipitation and no more distinctive motion characteristics. It also should be considered that on the pre-frontal side the flow is parallel to the front, i.e. a front approaching from North-West will have south-westerly flow

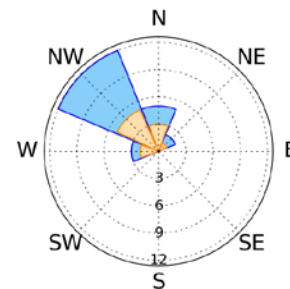


Figure 13. Approaching direction of cold fronts in winter for the Munich/Salzburg region, Blue: total number of events; orange: number of events being delayed/blocked by the Alps.

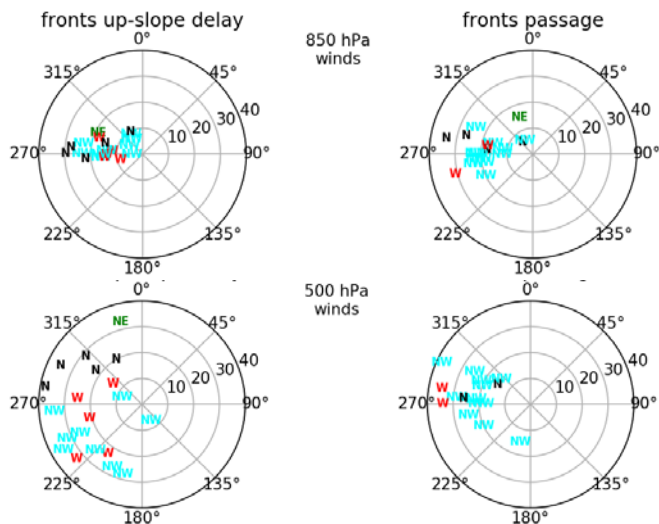


Figure 13. Wind direction for two levels (top row: 850 hPa; bottom row: 500 hPa) for situations with up-slope/delay and passage (left column: up-slope/delay; right column: passage) of 22 cold fronts events during winter. Labels (and colors) indicate the approaching direction of the frontal systems.

ahead of the front. A further investigation of propagation direction, motion vectors for those events, and wind field is ongoing.

VI. CONCLUSIONS

The four case studies used for verification show, that the values of verification scores depend greatly on the weather situation. Hence, no conclusion can be drawn by comparing the skill of forecasts made during different time periods. Based on visual comparison of cases in different weather situations, the Proesmans method was found out to produce the most reliable motion fields. However, the robustness of the method in cases of poor quality of input data (residual clutter) or missing data must be further improved. Verification of results with a statistically representing dataset remains to be made after the improvements have been implemented.

The stochastic ensemble method is clearly our preferred solution for producing probabilistic nowcasts, as it is assessing more sources of uncertainty than the simpler methods. Work is needed to improve the computational performance and to define the hardware requirements to calculate the nowcasts for real-time service.

Many of the methods for converting radar reflectivity to liquid water equivalent, snow depth and visibility introduced in the literature need such knowledge of microphysics which is not available operationally at the airports. We will continue following new scientific articles in the subject.

VII. FUTURE WORK

In this project, we have focused on radar-based methods due to their outstanding temporal resolution. In the possible follow-up projects, data fusion with other data sources such as numerical weather prediction should be considered, both to

extend the valid time and widen the available weather parameters.

ACKNOWLEDGMENT

The authors would like to thank colleagues at Helsinki University for fruitful co-operation. The PNOWWA project has received funding from the SESAR Joint Undertaking under the European Union's Horizon 2020 research and innovation programme under grant agreement No 699221.

REFERENCES

- [1] Andersson T. and K. Ivarsson, 1991: A model for probability nowcasts of accumulated precipitation using radar. *J Appl Meteorol* 30:135-141 DOI: [http://dx.doi.org/10.1175/1520-0450\(1991\)030<0135:AMFPNO>2.0.CO;2](http://dx.doi.org/10.1175/1520-0450(1991)030<0135:AMFPNO>2.0.CO;2)
- [2] Holmlund, K., 2000: The Atmospheric Motion Vector retrieval scheme for meteosat second generation. Proceedings of 5th International Winds Workshop, Melbourne, 28 Feb-3 March. Eumetsat.
- [3] Hohti H., J. Koistinen, P. Nurmi, E. Saltikoff, K. Holmlund, 2000: Precipitation Nowcasting Using Radar-Derived Atmospheric Motion Vectors. Proceedings of ERAD - the First European Radar Conference. Bologna, Italy.
- [4] Holmlund, K., 1998: The Utilization of Statistical properties of Satellite-Derived Atmospheric Motion Vectors to Derive Quality Indicators. *Weather and Forecasting*, 13, 1093-1104.
- [5] Barnes, S.L., 1964: A technique for maximizing details in numerical weather map analysis. *J.Appl.Meteor.* 3, 396-409.
- [6] Holmlund, K., 1999: The use of observation errors as an extension to Barnes interpolation scheme to derive smooth instantaneous vector fields from satellite-derived atmospheric motion vectors. Proceedings of the 1999 EUMETSAT meteorological satellite data users conference, Copenhagen, Denmark 6-10 September 1999 Eumetsat, EUM P26. 633-637.
- [7] Pulkkinen S., J. Koistinen, A.-M. Harri, 2016: Consistency-Driven Optical Flow Technique for Nowcasting and Temporal Interpolation. ERAD the 9th European Radar Conference
- [8] Proesmans, M. L. Van Gool, E. Pauwels, A. Oosterlinck, 1994: Determination of optical fow and its discontinuities using non-linear diffusion. In 3rd European Conference on Computer Vision, ECCV'94, 1994, Vol. 2, pp. 295-304.
- [9] Jolliffe, T. and D.B. Stephenson, 2012: *Forecast Verification: A Practitioner's Guide in Atmospheric Science*. 2nd Edition. ISBN: 978-0-470-66071-3
- [10] ICAO, Annex 15: SNOWTAM format. Available online e.g. <http://www.skybrary.aero/bookshelf/books/2361.pdf>
- [11] Rasmussen R. M., J. Vivekanandan J. Cole, B. Myers, C. Masters, 1999: The Estimation of Snowfall Rate Using Visibility. *J. Appl. Meteor.*, 38, 1542-1563.
- [12] Boudala F.S. and G.A. Isaac, 2009: Parametrization of visibility in snow: Application in numerical weather prediction models. *Journal of Geophysical Research*, vol. 114, D19202.
- [13] Dixon M., R.M. Rasmussen, S. Landolt, 2004: Short-term Forecasting of Airport Surface Visibility Using Radar and ASOS. 11th Conference on aviation, range and aerospace, Hyannis, MA, 4-7 Oct 2004.
- [14] Ylinen, K, 2013: Näkyvyyden ja tutkakaiuin voimakkuuden välinen riippuvuus lumisadetapaüksissa (Relationship of visibility and radar reflectivity in snowfall). BSc Thesis, Helsinki University, in Finnish.
- [15] Schumann, U., 1987: Influence of Mesoscale Orography on Idealized Cold Fronts. *J. Atmos. Sci.*, 44, 3423-3441, [https://doi.org/10.1175/1520-0469\(1987\)044<3423:IOMOOI>2.0.CO;2](https://doi.org/10.1175/1520-0469(1987)044<3423:IOMOOI>2.0.CO;2)
- [16] Volkert H., L. Weickmann, A. Tafferner, 1991: The Papal front of 3 May 1987: A remarkable example of fronto-genesis near the Alps. *Quart J Roy Meteorol Soc* 117, 125-150.